# Study on Structure and Orientation Action of Polyurethane Nanocomposites

**Xinhua Dai, Jain Xu,* Xinglin Guo, Yonglai Lu, Deyan Shen, Ning Zhao, Xiangdong Luo, and Xiaoli Zhang**

*State Key Laboratory of Polymer Physics and Chemistry, Institute of Chemistry, Chinese Academy of Sciences, Beijing 100080, China*

*Received January 13, 2004; Revised Manuscript Received May 12, 2004*

ABSTRACT: Segmented polyether−polyurethane (PU)/montmorillonite nanocomposites have been synthesized with poly(tetramethylene glycol), 4,4-diphenylmethane diisocyanate, propylenediamine, and montmorillonite. The nanoscale silicate layers are intercalated or exfoliated in the PU matrix, which are characterized by X-ray diffraction pattern and transmission electron microscopy. The PU/montmorillonite composites have been investigated by FT-IR dichroism during the stretching process in order to study the hard and soft chain orientation, hydrogen bonding, and strain induced by crystallization of the soft segment chains in PU. DSC experiment indicates that the soft phase $T_g$ increases with the montmorillonite content. The mechanical analysis showed that tensile strength,Young's modulus, and elongation at break increase markedly, 1700% elongation at break for the composite containing 2.0 wt % montmorillonite.

## Introduction

Polyurethanes, a category of synthetic polymers discovered in the 1930s, are utilized as an elastomer with their higher performances.[1] They have a variety of applications due to their unique properties, such as high strength, high hardness, high modulus, and high elongation at break. However, so far, there is not the combination of these properties for any other commercial products. Their ability to be fabricated by almost any of the conventional technologies has also been important in leading to their present universal applications.

Recently, intercalation of organophilic silicate layers or clay in several polymers has been introduced as an attractive route, leading to versatile polymer composites especially containing nanoscale silicates with high aspect ratio.[2−8] A few examples of using special intercalated organophilic silicate layers as filler in PU were described in these previous studies.[9−12] Nanocomposites of PU/montmorillonite were prepared with nanoscale organo-clay, in which the mechanical properties of the PU nanocomposite are improved. However, the information about the silicate−PU "interaction" and its mechanics has still been insufficient, although FT-IR spectra of polyurethane are sensitive to microdomain organization and the hydrogen bonding of urea and urethane.[13−15]

In this work, we have prepared the PU/montmorillonite nanocomposites by the solution-intercalation technique.[16] The alignment studies of PU nanocomposites with montmorillonite contents were carried out to look at the orientation action, the hydrogen-bonding property, and the strain-induced crystallization of polymer chains, in which the FT-IR dichroism was first applied to characterize the microstructure of the PU/montmorillonite nanocomposites. Consequently, the correlations between the structure and mechanical properties of prepared PU/montmorillonite nanocomposites were discussed, which have much excellent mechanical properties than those of the polymer matrixes, especially elongation at the break.

* Corresponding author: Fax 86-10-82619667; Tel 86-10-82619667; e-mail jxu@iccas.ac.cn.

## Experimental Section

**Materials.** Sodium montmorillonite (silicate layers or clay) with a cation-exchange capacity (CEC) of 100 mequiv/100 g and an interlayer spacing of 1.25 nm was kindly supplied by Laboratory of Engineering Plastics, Chinese Academy of Sciences. 1,3-Propylenediamine (PDA, 99%, Fisher) and *N*,*N*′-dimethylformamide (DMF) were stored in 4 Å molecular sieve for 1 week and subsequently distilled prior to use. Poly(tetramethylene glycol) (PTMG, $M_n = 2000$, B.F. Goodrich Co.) was dehydrated in a vacuum oven at 60 °C for 2 days. 4,4-Diphenylmethane diisocyanate (MDI, Yantai Synthetic Leather General Factory) was heated to 60 °C and kept at that temperature for 2 h and then filtered through a heated filter. Cetyltrimethylammonium bromide (CTAB, Sigma) was used as received.

**Preparation of Organophilic Montmorillonite.** To disperse montmorillonite in a polyurethane matrix, it was necessary to first replace the hydrophilic inorganic exchange cations with more organophilic alkylammonium ions. 12.04 g of Na montmorillonite was added to 500 mL of an aqueous solution of CTAB (0.5 wt %). The suspension was vigorously stirred for 4 h at 80 °C. A white solid product formed after filtration was collected and repeatedly washed by deionized water and acetone and subsequently dissolved in 200 mL of DMF at 90 °C. Finally, poly(tetramethylene glycol) (PTMG, 2.01 g) was added and vigorously stirred for 3 h at 90 °C. After removal of the solvent by evaporation under reduced pressure, the solid product was dried in a vacuum oven at 70 °C for 10 h. The obtained organophilic montmorillonite was ground and screened with a 325 mesh sieve.

**Preparation of the PU Nanocomposites.** A polar solvent can be used to synthesize intercalated polymer montmorillonite nanocomposites. Here, the "solution polymerization"[16] approach is used to prepare the composites. To investigate the effect of montmorillonite content on the mechanical properties and microstructure of PU/montmorillonite nanocomposites, three concentrations of montmorillonite were used: 1.0, 2.0, and 4.0 wt %. The synthetic procedures were described as follows. First, in a 500 mL three-necked flask was placed 120 mL of DMF, and an appropriate amount of organic montmorillonite was added and stirred at 80 °C under flowing $N_2$ gas until the solution became homogeneous. Second, MDI and PTMG at a molar ratio of 2:1 were dissolved in the aforemen-

10.1021/ma049900g CCC: $27.50 
Published on Web 07/02/2004

**Table 1. Composition, Apparent Number Molecular Weight, and Distribution of PU and PU/Montmorillonite Nanocomposites**

| | molar ratio (MDI/PDA/PTMG) | clay content (wt %) | $M_n$ | $M_w$ | $M_w/M_n$ |
|---|---|---|---|---|---|
| PU | 2/1/1 | 0 | $5.74 \times 10^4$ | $5.99 \times 10^4$ | 1.04 |
| I | 2/1/1 | 1.0 | $5.63 \times 10^4$ | $5.97 \times 10^4$ | 1.06 |
| II | 2/1/1 | 2.0 | $5.57 \times 10^4$ | $5.85 \times 10^4$ | 1.05 |
| III | 2/1/1 | 4.0 | $5.39 \times 10^4$ | $6.25 \times 10^4$ | 1.16 |

tioned solution, and the solution was maintained at 80 °C for 3 h to form a prepolymer which was then cooled. Third, 1,3-propylenediamine (at an equal molar of PTMG) was added to the prepolymer with stirring at 15 °C for 1 h to ensure the completion of the reaction. Finally, the samples for mechanical property testing were prepared by casting the solution of 1.0% PU or PU nanocomposites in DMF on a circular quartz mold, and the detailed approach can be found in the WAXD experiment. The films thickness was adjusted by the amount of the cast solution. Samples used in elongation test were cut to standard dumbbell shape. In the sequence of the increase in the content of organic montmorillonite, the samples obtained are denoted as samples I, II, and III. Pure PU was also synthesized by the same procedures but without addition of organic montmorillonite. The composites of the PU/montmorillonite nanocomposites are given in Table 1.

**Polymer Recovery for Molecular Weight Determination.** The synthesized PU/montmorillonite nanocomposites (0.2 g) was added to 3.0 mL of toluene with stirring for 3 h at room temperature. After filtration, a clear PU/montmorillonite solution was obtained. The clear PU solution was then gradually dropped under stirring to 4 mL of 1.0% LiCl/DMF solution. The finished mixture was placed in room temperature for 48 h for performing the reverse ion-exchange reaction. After the ion exchange, the solution was centrifuged at 5000 rpm for 8 min. The supernatant liquid was distilled under reduced pressure to remove the solvent, and the pure PU recovered from nanocomposites was obtained.

**Characterization.** Wide-angle X-ray diffraction (WAXD) analysis was performed using a Japan D/MAX.RB diffractometor with Cu K$\alpha$ radiation ($\lambda = 0.1518$ nm) at a generator voltage of 40 kV and a generator current of 100 mA. The scanning was in 0.02° steps at a speed of 2°/min, beginning with $2\theta$ value at 1.5°. The experiment was carried out on the films in two different directions normal and parallel to composite films. Samples for the WAXD experiments were prepared as follows: the as-polymerized solution (~1.0 wt %) were poured into shallow circular quartz molds and placed low vacuum (about 10 in. Hg) under 65 °C and maintain at this temperature to remove the trace of DMF. Films were on the order of several decades to 100 $\mu$m thick. The samples were transparent to visible light. A single film was used to test WAXD in the normal direction. The films were stacked to create a thickness suitable for WAXD experiment in the parallel direction to composite films. The films have a high affinity for each other, so the films adhered well.

Transmission electron microscopy (TEM) observation was undertaken on a H-800 transmission electron microscope to acquire a direct visualization of the particular layer characteristics of the nanocomposites. Ultrathin sections of bulk samples were prepared at −100 °C using a Leica Ultracut UCT with an EMFCS cryo-attachment. The sections were transferred from the diamond knife edge to 200 mesh Cu grids. The gel permeation chromatography (GPC) measurements were performed on pure PU and PU recovered from PU/montmorillonite nanocomposites. The apparent molecular weights were determined by a Waters 510 GPC using DMF as the solvent at 60 °C. The calibration curves for GPC were obtained by applying polystyrene standards.

Survey IR spectra of samples were obtained with a Bruker EQUINOX 55 FTIR spectrometer equipped with a liquid nitrogen cooled MCT detector. Spectrum resolution is 4 $cm^{-1}$, and every spectrum is 32 scans averaged. The sample films were prepared by dropping 1.0% PU or PU/montmorillonite solution onto quartz slide, placed low vacuum (about 10 in. Hg) at oven temperature of 65 °C, and maintained at this temperature to remove the trace of DMF. If necessary, the amount of polymer solution was adjusted to yield films of an appropriate thickness required to stay within the range of Beer's law. The films were peeled off from quartz slide and cut in the form of dumbbell shape.

Infrared dichroism measurements were obtained by coupling the FT-IR with a stretching device, which elongated the sample film from both ends simultaneously. A Perkim-Elmer gold-wire grid polarizer was inserted between the sample and detector and set at 0° or 90° for recording $A_{||}$ or $A_{\perp}$, respectively. Five minutes of stress relaxation[15] was allowed before the polarized spectra were recorded.

The theory and application of infrared dichroism have been documented elsewhere.[17,18] In multiphase polymer systems, infrared dichroism can be used to study the deformation of chain segments in each domain by following the absorptions of functional groups residing on segments in different phases. In the present study the segmented polyether−polyurethane is a kind of block copolymer of the type $(AB)_n$ composed of alternating soft and hard segments along the molecular chain. The hard segments are based on diisocyanate and diamine, while the soft segments are typically polyether. Analysis of the IR peak intensities similar to that of Seymour et al.[19] was performed to determine as the change in the concentration of hydrogen-bonded functional groups with deformation. Assuming cylindrical symmetry, it can be shown that the average absorbance $A$ is given by eq 1 for a uniaxially oriented sample. This relation has been obtained through the calculation of specific absorbance as it should be independent of the orientation of the absorbing groups.

$$A = {}^1/_3(2A_{\perp} + A_{||}) \tag{1}$$

Thermal analysis was conducted by DSC of a Mettler Toledo 822$^e$ in the temperature range −130 to 150 °C at a heating rate of 20 °C/min under a $N_2$ purge. The empty-pan DSC baseline was subtracted from each sample's thermogram by means of a scanning auto zero module, and the data were further normalized to an equivalent sample weight. Separate high-temperature DSC experiments were carried out on the as-cast samples to characterize hard segment melting.

The tensile properties were measured by means of stress/strain tests with an Instron-1122 machine. The experiments were conducted at room temperature with the deformation rate of 100 mm/min.[11,12,20] The initial length and thickness of the samples are 20 and 0.1 mm, respectively. For each data, five samples were tested and the average value was taken.

## Results and Discussion

The degree of silicate layers dispersion and delamination is usually obtained by X-ray diffraction measurements. Generally, the intense reflections within the range of 1.5°−10° ($2\theta$) indicate the formation of an ordered intercalated system with alternating polymer/silicate layers.[21−24] In the completely delaminated hybrids, silicate layers with a thickness about 1 nm are relatively homogeneously dispersed in the polymer matrix. WAXD patterns give no distinct features in the low range of $2\theta$ due to the loss of structural integrity. As shown in Figure 1A of WAXD patterns of untreated and treated montmorillonite, the values of $d$ spacing[8] of the pristine montmorillonite and the treated montmorillonite are 1.25 and 1.95 nm, respectively. It means that the silicate layer galleries in the montmorillonite are effectively intercalated by poly(tetramethylene glycol). The normal and parallel WAXD patterns of pure PU and PU/montmorillonite nanocomposites films exhibit the same diffraction features as shown in Figures 1B and 1C. Therefore, it indicates that there is no preorientation for PU/montmorillonite nanocomposites

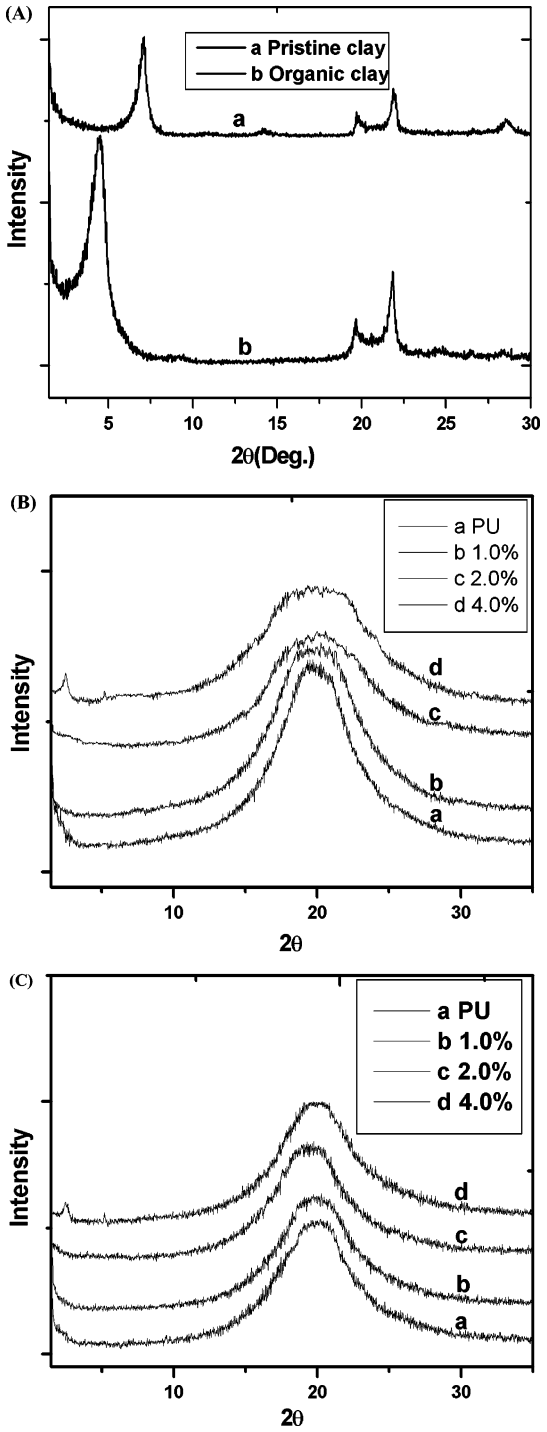


**Figure 1.** (A) XRD patterns of untreated montmorillonites (curve a) and treated montmorillonites (curve b). The diffraction patterns are given by X-ray normal to films (B) and parallel to the films (C). The montmorillonite weight percentage in PU and its nanocomposites are curve a, 0.0 wt %; curve b, 1.0 wt %; curve c, 2.0 wt %; and curve d, 4.0 wt %.

samples obtained by casting from the solution. The pure PU exhibits an amorphous halo near $2\theta = 20°$, consistent with the result of Runt et al.,[25] and is found at the same location for all of the composites. Again in Figure 1B,C, it can be seen that no characteristic diffraction peaks appear in the range of $2\theta$ from 1.5° to 10° in pure PU and samples I and II, implying that PU is intercalated into layered silicates. The increase in interlayer distance of the silicates renders the silicates broken down into nanoscale building blocks and then exfoliated

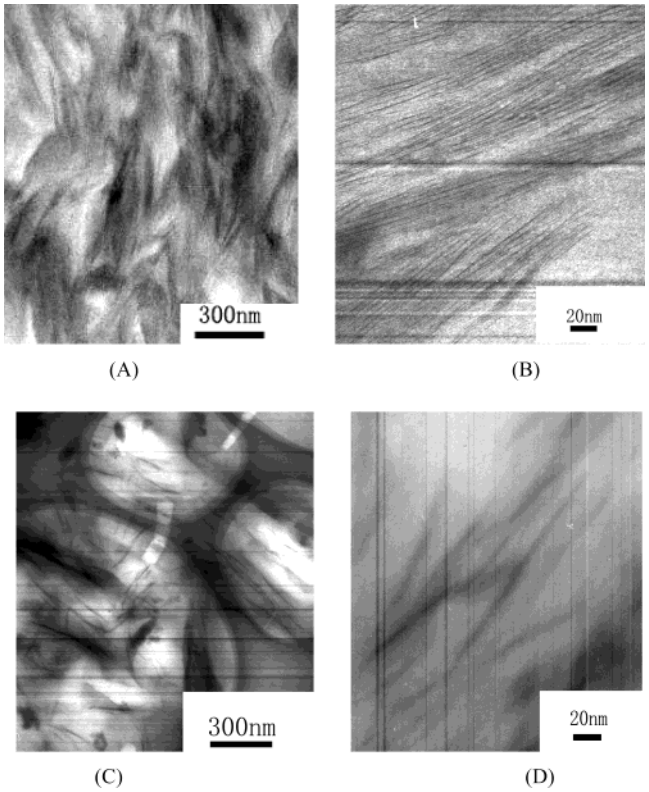


**Figure 2.** TEM micrographs of PU/montmorillonite nanocomposites with clay contents. Low magnification (A) and high magnification (B) of sample III (4.0 wt %). Low magnification (C) and high magnification (D) of sample II (2.0 wt %).

and dispersed in PU matrix. However, with an increase of the organic montmorillonite concentration, there still are some clay amines assembled together. The *d* spacing value of clay in sample III (4.0 wt % montmorillonite) is tested to be 3.9 nm. At a higher content of silicate layers, a complete and effective entry of monomers into the organically modified silicate layers is very difficult.[26] Because the entropy gained by desorption of solvent molecules is not enough for all monomers to intercalate, the XRD results gave useful information. Further, conventional TEM can provide more direct information on morphology in real space. The TEM images have been obtained for samples II and III (Figure 2). Parts A and B of Figure 2 present the TEM images of sample III in a low and high magnification, respectively. Both images show an intercalated structure and ~4 nm of distance among clay layers. This result was also proved by XRD in curve d of Figure 1B,C. In Figure 2C,D, the silicate layers in sample II (2.0 wt % montmorillonite) are disordered and dispersed relatively homogeneously in polyurethane, which indicated that the organic montmorillonite is almost exfoliated and dispersed in nanoscale into the PU matrix. However, not all clay platelets are exfoliated into single platelet, in which there still exist some of the coherent stacking of several to decade layers with intercrystallite gaps from several nanometers to tens of nanometers within the primary particles. It might be deduced that the absence of the characteristic diffraction peaks of curves b and c in Figure 1B,C arises from the random dispersion of the primary particles, different distances among clay, and their heterogeneous microstructure in Figure 2.[27]

The apparent molecular weights of pure PU and recovered PU from its nanocomposites are given in Table 1. The apparent molecular weight of PU recovered

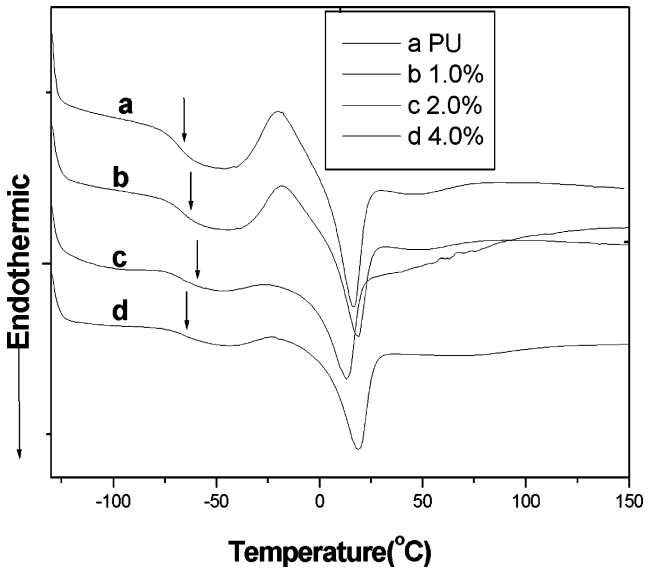


**Figure 3.** DSC curves of the soft segment $T_g$ of PU and PU/montmorillonite nanocomposites.

from PU/montmorillonite composites showed a slight decrease as compared to that of pure PU but less than 10%. It indicated that the PU molecular chain lengths were not affected by the presence of the silicate layers. This results consistent with the result by Wei et al.[20] In addition, the molecular weight distribution of PU/clay composites did not change, though there existed different reactivity of the polymer within the layers. This phenomenon is interesting and requires further investigation.

In Figure 3, the changes of the glass transition temperature ($T_g$) for pure PU and PU nanocomposites with the montmorillonite contents are given. The primary relaxation observed at −80 to −50 °C is designated as the α relaxation and has been assigned to the glass transition of the PTMG soft segment. With increasing the organic clay content, the $T_g$ peak moved somewhat higher and the intensity of peak become weak. This is tentatively attributed to the confinement of the segmental motions of intermolecular chains of the polymer within the clay galleries.[28] The other cause can be attributed to the restricted chain mobility in the interfacial layer, in which polymer chains are effectively anchored or attached to the silicate surface. These anchored polymer chains form an interphase region where the segment relaxation is slower than in the bulk. The restricted relaxation behavior for the polymer nanocomposites with intercalated and exfoliated silicates depended primarily on the exfoliation extent of the layered silicates and the interaction strength between the silicate surfaces and the PU macromolecules. Thus, a system with fully exfoliated silicate dispersion and strong interactions is expected to exhibit slow relaxation behavior, while a system with intercalated silicates and relatively weak interaction should display fast relaxation dynamics. In addition, the overall relaxation behavior of the nanocomposites depends still on the ratio of restricted and unrestricted macromolecular segment numbers, related with the clay contents and its dispersion morphology.[29] Here sample II with almost exfoliated clay in PU matrix and bonded with polymer segments through hydrogen-bonding interaction (this result will be discussed later) had the highest $T_g$ and weaker peak intensity in our study.

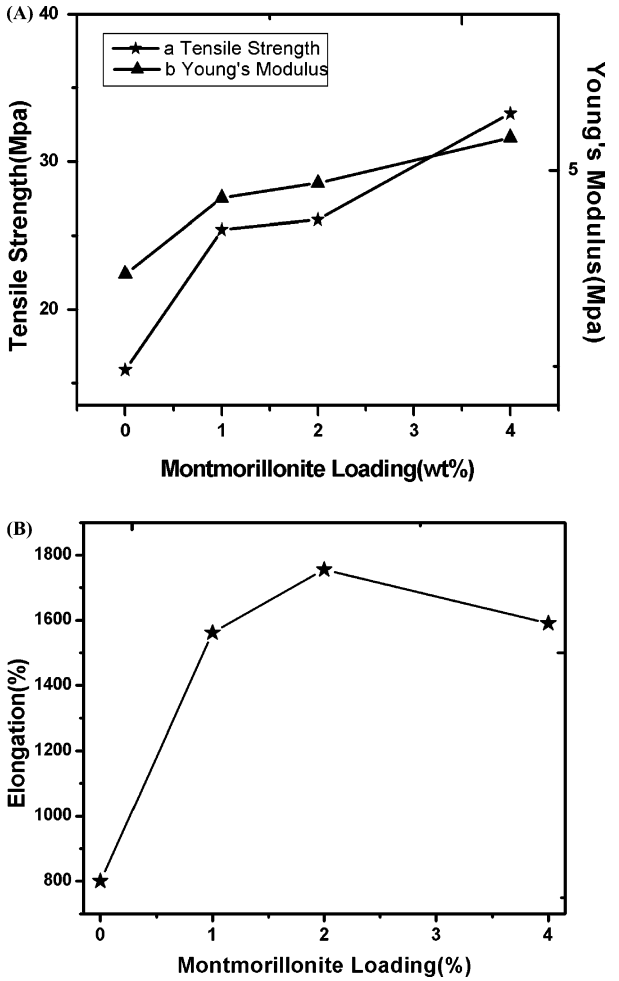


**Figure 4.** Tensile strength, Young's modulus (A), and elongation at the break (B) of PU/montmorillonite nanocomposites vs organic montmorillonite contents.

The endo- and exotherms between −25 and +25 °C in polyurethane were reported.[15] The low-temperature endotherm is attributed to the melting of metastable PTMG crystallites. The higher temperature melting peak is associated with crystalline PTMG segments closer to their equilibrium state. As shown in curve a to curve d of Figure 3, the endotherm peak area of the PTMG melting in the composites is relatively reduced with clay intercalation and suggests that part of the PTMG resides in the montmorillate galleries. The change in the melting action of these samples has been attributed to imperfect crystals in the constraining environment of the interlamellar gallery.[30,31] Clay appears to restrict the chains relaxation and to disrupt the crystallization of the soft segment, which is induced by stress (also see Figure 10).

In both pure PU and PU/montmorillonite nanocomposites, $T_g$ of the hard segments and any crystallization as well as melting transition were not detected. This is in accord with the result of ref 15. It might be due to the low content of hard segments (about 20.0 wt % in our work) and greater soft/hard segments mixing percent in these systems studied, which interferes with the crystallization of hard segment.

Figure 4 compares the mechanical properties of PU/montmorillonite nanocomposites with those of pure PU sample without any processing aids or other additives. The nanocomposites show an improvement in elasticity due to the incorporation of the organic montmorillonite.

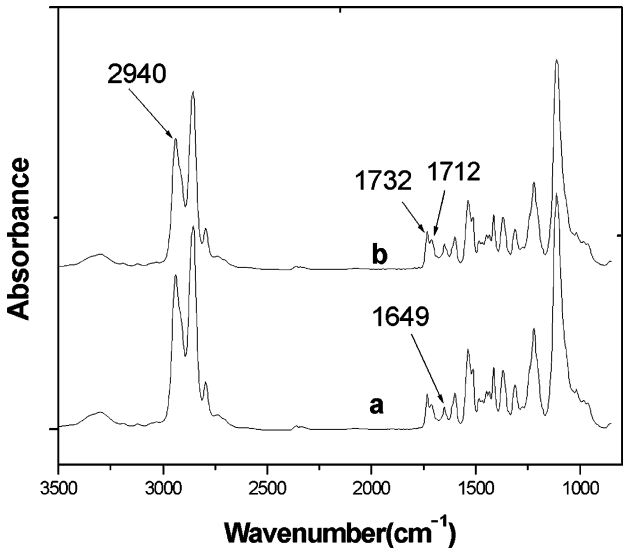


**Figure 5.** FT-IR spectra of pure PU (a) and PU/montmorillonite nanocomposite (b).

With an increase in the amount of organic montmorillonite, both the Young's modulus and tensile strength at break are gradually increased, as shown in Figure 4A. The enhancement in Young's modulus and tensile strength is directly attributed to the reinforcement coming from the dispersed stiff nanolayers of silicate clay.[9] From Figure 4B, it can be found that the elongation at break is obviously improved in the presence of exfoliated silicate layer in nanoscale. It is much surprising and very interesting that sample II (2.0 wt % montmorillonite) displays an excellent elongation behavior, in which the largest value of elongation at break is about 1700%. As is well-known, an increase of material tensile strength results usually in the decrease of its tensile elongation for most polymers or polymer composites. However, by means of intercalated silicate layers in nanoscale, both elongation at break and tensile strength of the PU nanocomposites increase simultaneously in our research.

**Orientation of PU Segment.** FT-IR dichroism experiments are conducted to study in situ the microstructure change of the PU/montmorillonite and pure PU during the elongation process. Figure 5 shows the FTIR spectra of pure PU and its composite samples recorded at room temperature. It is noted that the band positions of distinctive functional groups of the pristine PU are identical to those of the PU/montmorillonite nanocomposites, confirming that the chemical structures of PU do not alter in the presence of silicate layers.[11] From Figure 5, spectral intensity changes of the PU/montmorillonite can be clearly observed in the regions at 3500−3200 $cm^{-1}$ (N−H stretching mode) and 1780−1600 $cm^{-1}$ (C═O stretching mode). Band assignments of characteristic groups in the composites are listed in Table 2.

According to Wang and Cooper's study,[15] several functional groups were used to follow the segmental orientation in the domains of the soft and hard segments for the PU/montmorillonite samples. They include (1) the average behavior of the C−H stretching band ($f_{2940}$), which is a measure of the soft segment orientation, (2) the C═O bond at 1732 $cm^{-1}$ ($f_{1732}$), which is a measure of the average orientation of the non-hydrogen-bonded urethanes either at the hard domain interfacial zone or of hard segments in the polyether matrix, (3) the

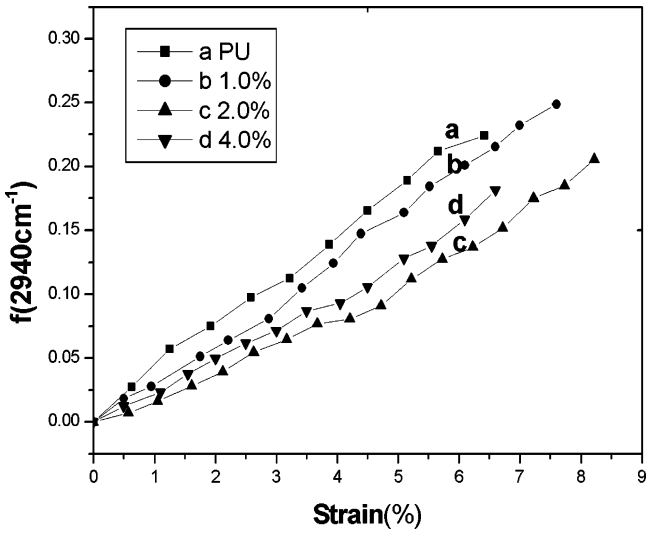


**Figure 6.** Orientation function vs strain of $CH_2$.

**Table 2. Assignments of the Absorption Bands in FT-IR Spectra of the Pure PU and PU/Montmorillonite Nanocomposites**

| freq ($cm^{-1}$) | assignment | domain origin |
|---|---|---|
| 3480 | $\nu$(NH), free | hard segment |
| 3320 | $\nu$(NH), hydrogen-bonded | hard segment |
| 2940 | $\nu(CH_2)$ | soft segment |
| 1732 | $\nu$(C═O), free urethane carbonyl | hard segment |
| 1712 | $\nu$(C═O), hydrogen-bonded urethane carbonyl | hard segment |
| 1649 | $\nu$(C═O), hydrogen-bonded, ordered urea carbonyl | hard segment |
| 997 | $\nu$(C−O−C), ether group | soft segment |

C═O absorption band at 1712 $cm^{-1}$ ($f_{1712}$), which follows the orientation of hydrogen-bonded urethane at the interface, and (4) the C═O band at 1649 $cm^{-1}$ ($f_{1649}$), which is a measure of the orientation of urea linkages within the hard domain. The most important parameters involved in infrared dichroism measurement are the structural absorbance, which is defined as eq 2. The dichroic ratio $R$

$$R = A_{\parallel}/A_{\perp} \tag{2}$$

and the orientation function

$$f = 2(R - 1)/(R + 2)[3(\cos\theta)^2 - 1] \tag{3}$$

Here $A_{\parallel}$ and $A_{\perp}$ are the absorbance of a band measured with incident light polarized parallel and vertical to stretching direction, respectively. $\theta$ is the angle of a transition moment of a vibrational mode to the molecular chain axis. The transition moment vectors of the C−H, C═O, and N−H functional groups were assumed to be respectively 90°, 78°, and 90°[15] to the chain axis.

Figure 6 shows the typical relationship between the orientation function ($f$) and the elongation percent for pure PU and PU composites. Upon deformation, the soft segments as monitored by $f_{2940}$ orient into the stretch direction. Introducing of the silicate layers effects the orientation of the soft segments. The soft segments orientation of the composites ($f_{2940}$) was found to be lower than that of the pure PU. In addition, as the clay content was increased, $f$ values of soft segment were lowered. It means that the orientation of the soft segments can been obstructed by the clay.

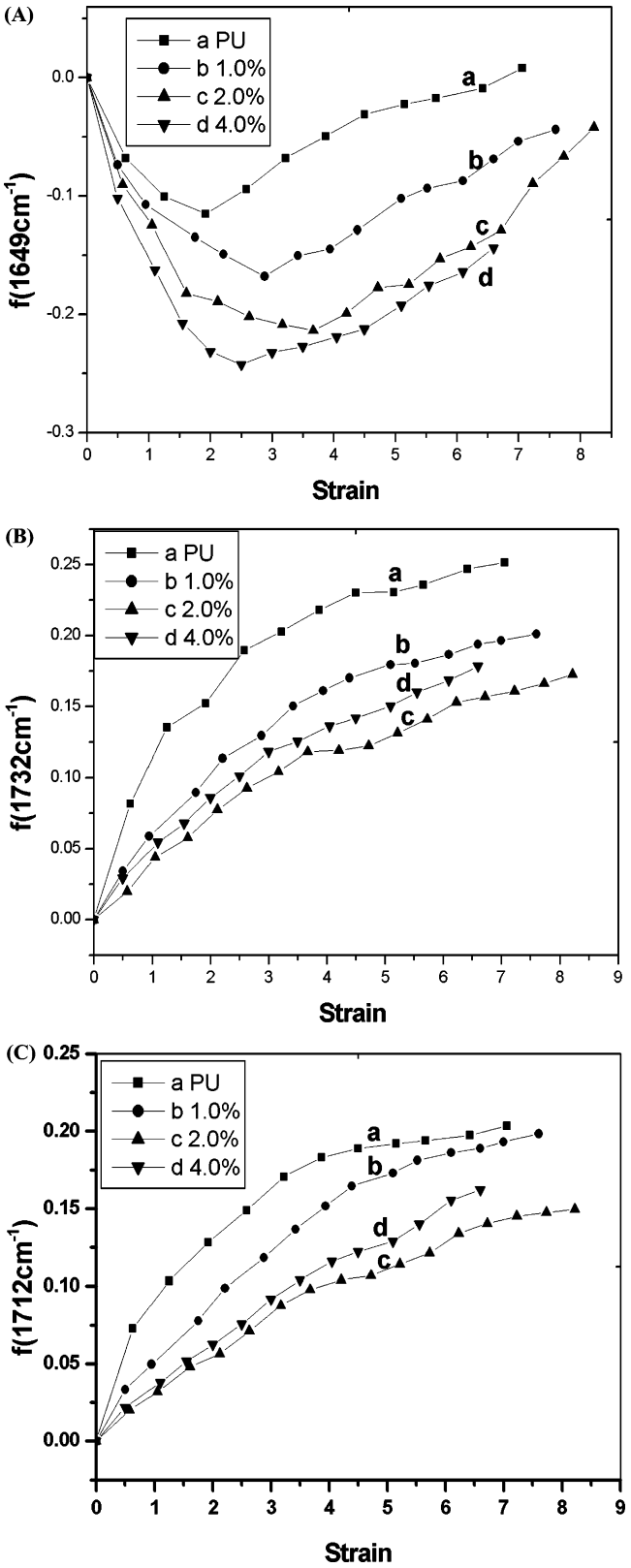


**Figure 7.** Orientation function of C═O 1649 $cm^{-1}$ (A), 1732 $cm^{-1}$ (B), and 1712 $cm^{-1}$ (C) vs strain.

The orientation behavior of the hard segments is more complicated as shown in Figure 7. A negative value of $f_{1649}$ indicates that the hard segments within the domains first orient transverse to the stretch direction in Figure 7A. In contrast, both the urethane carbonyl orient positively (Figure 7B,C), suggesting that hard segments at the interface become aligned into the stretch direction. In Figure 7A, it is obvious that the orientation function for all PU/montmorillonite samples becomes smaller than that of pure PU, suggesting the mobility of molecular chains was influenced by the silicate layers with relative rigidity property. Moreover, sample III (4.0%) had the smallest orientation magnitude. The mobility of the hard segments was retarded mostly by the rigid silicate layers. From these phenomena, it is reasonable that the tensile strength of sample III is higher than other samples. A negative value of $f_{COB,UA}$ indicates that the hard segments within the domains first orient transverse to the stretch direction and then carbonyls orient positively, suggesting that hard segments of urea linkages within the hard domains become aligned into the stretch direction.[15] At low strains the deformed PU hard segment domains maintain most of their structural integrity and retain the three-dimensional inter-urea hydrogen bonds. At higher strains some of the lamellae begin to disintegrate, ultimately allowing hard segment chain orientation parallel to the stretch direction.

Ishihara and co-workers[32] showed the behavior of carbonyl of the urea bonding with the elongation. During deformation process the carbonyl of the urea bonding action may suggest that the breakage of inter-urea hydrogen bonding begins at the elongation where the transverse orientation reaches a maximum; that is to say, the values of $f_{COB,UA}$ reach the minimum values. So the elongation at the minimum values of $f_{1649}$ may serve as a character when the disruption of the hard segment domains takes place. The maximum negative chain orientation depends on the stability of the lamellar morphology of the hard domains in these samples. The hard segment structure of the PU polymers plays an important role in their phase separation, and the phase separation acts physical cross-link effects, which results in the unique mechanical property of PU and PU composites.

A higher value of strain at this minimum $f_{1649}$ was observed for sample II compared to other samples. The elongation at break at room temperature (Figure 4B) also shows a trend consistent with the orientation behavior. In fact, there are higher elongation at the break and bigger strain of the PU composite corresponding to the minimum of $f_{1649}$. That is to say a high value of elongation at break correlates with the higher strain value where the $f_{1649}$ reaches minimum. This mainly comes from the relatively steady structure of the hard segments.

Figure 7B presents the orientation of C═O bond at 1732 $cm^{-1}$ ($f_{1732}$). The orientation of this group was retarded, which located at the interfacial zone or of hard segments in the PU matrix. The change magnitude of orientation function for sample II is the smallest. The silicate layers were exfoliated in the PU matrix that constructed large interfacial areas. The mobility of the hard segments, located at this interfacial zone, was retarded mostly by the rigid silicate layers. For sample III the segment chains were obstructed only by the partly intercalation of the silicate layers, so the orientation change magnitude was faster than that of sample II. Figure 7C presents the orientation of hydrogen-bonded urethane ($f_{1712}$) at the interface. The change magnitude of orientation function is similar to the action of $f_{1732}$. During the stress relaxation period following sample stretching, the orientation of the chain segments will be influenced by molecular relaxation process. The

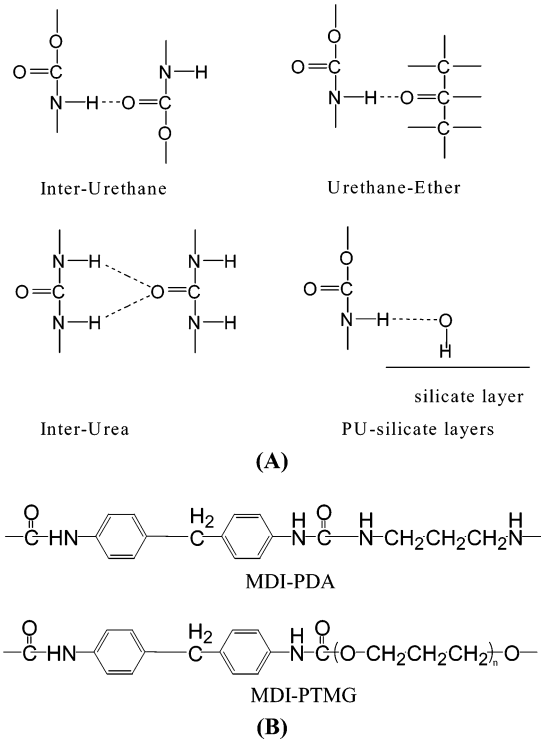


**Figure 8.** (A) Hydrogen-bonding interaction in PU and PU/montmorillonite nanocomposites. (B) The unit structures of PU.

extent of segment relaxation was affected by the relative rigidity of the corresponding phase domain at the testing temperature (room temperature for this work). Thus, the orientation ($f_{1712}$) was lower than the orientation of the non-hydrogen-bonded urethanes ($f_{1732}$).

For every orientation−strain relationship plotted in Figures 6 and 7, the orientation function for these samples decreases with increasing clay content; that is, the ability of the polymer orients or remains oriented state at 5 min of time scale in our strain experiment. It is obvious that the presence of the silicate layers affects their orientation of the two domains response to stretching.

**Hydrogen Bonding of PU Segment.** It is generally accepted that hydrogen bonding between functional group is very closely related to the phase separation,[33−35] and the degree of phase separation plays a key role in PU mechanical properties. The hydrogen bonding in the PU/montmorillontie is very complex.[32,36] As shown in Figure 8A, multiple hydrogen bonds may be formed between two kinds of proton donators (urethane N−H and urea N−H groups) and four kinds of proton acceptors (urethane C═O, urea C═O, ether C−O−C groups, and the oxygen of the hydroxy groups −OH on silicate layers). The unit structures of the PU copolymer are shown schematically in Figure 8B. The urea groups only exist in the interior of hard segments, and they were formed by reacting PDA with MDI. Urethane groups, however, exist mainly on the boundaries between the hard segments and the soft segments. The urea hydrogen bonds were sensitive to the morphological changes in hard segment domains, while the urethane hydrogen bonds were more sensitive to those on phase bond boundaries.

The carbonyl region in the FTIR spectra is most applicable to analysis of the hydrogen-bonding properties.[35−39] The stretching vibration mode of the urethane carbonyl group in the PU/montmorillonite composite can be observed from 1780 to 1700 $cm^{-1}$. The 1732 $cm^{-1}$ band is caused by the free of carbonyl of the urethane group, and the band at 1712 $cm^{-1}$ is associated with the hydrogen-bonded carbonyl of the urethane group. The relative absorbance of the double carbonyl peaks should serve as an index that the group participates in hydrogen bonding. The hydrogen-bonding index, $R$, may be defined as the ratio of the absorbance $A_{1712}/A_{1732}$.[15,19] The greater value of $R$ indicates increased participation of the carbonyl group in hydrogen bonding. Within the approximation of the baseline method, the hydrogen bond index may be expressed as

$$R = C_{\text{bonded}}\epsilon_{\text{bonded}}/C_{\text{free}}\epsilon_{\text{free}} = A_{1712}/A_{1732} \qquad (4)$$

Here $A$ is the absorbance of characteristic band, $C$ is the concentration, and $\epsilon$ is the extinction coefficient of bonded and free carbonyl groups. Knowing the two extinction coefficients, the ratio of bonded to free functional groups could be calculated. The value of $\epsilon_{\text{bonded}}/\epsilon_{\text{free}}$ is 1.0−1.2. Here 1.2 is taken as the value of $\epsilon_{\text{bonded}}/\epsilon_{\text{free}}$. Table 2 shows assignments of the absorption bands in FT-IR spectra of the pure PU and PU/montmorillonite nanocomposites.[15]

For simplicity in data manipulation, the straight baselines were used, and the corresponding peak height was taken to represent the specific polarized infrared absorbance in this work. The data were obtained directly from IR absorbance spectra. Since all of the IR spectra for PU and PU nanocomposite samples were analyzed on the same basis, the data presented in this section are assumed to have semiquantitative significance because analysis involving peak deconvolution was not applied.

Figure 9A shows a comparison of the carbonyl stretching region with no stretching samples in order to show the changes of hydrogen bonding. According to eqs 1 and 4, the hydrogen-bonding changes of urethane carbonyl, as a function of the concentration of clay in these samples, are presented in Figure 9B. The degree of hydrogen bonding of urethane carbonyl increases with the clay ratios in the PU matrix. Sample II has the maximal increase in the hydrogen-bonding index of the carbonyl group. This phenomenon can be manifested by a close observation of the sample's morphology. As discussed above, the carbonyl of the urethane exists mainly on the boundaries between hard and soft segments. The nanometer-scale silicate layers dispersed in PU result in some interfacial areas, on which the hydroxyl groups can form hydrogen bonding with either the hard or the soft segments of PU. Therefore, the hydrogen-bonding index for PU/montmorillonite nanocomposites is bigger than that of pure PU. These exfoliated silicate layers in sample II give larger interfacial areas, on which hydroxyl groups of the silicate layers can form more hydrogen bonding with PU (this result responding with the $T_g$ of materials shown in Figure 3). For sample III, the intercalation of the silicate layers by the PU decreased when the amount of clay increased, evidenced in the TEM micrographs in Figure 2A,B. Hence, the extent of the formation of hydrogen bonding diminished as compared to sample II.

According to the values of $R$, the degree of hydrogen bonding in urethane increases with the clay content. Because the existence of hydrogen bonding enhances the effects of physical cross-linkers and filler in the composite, the tensile property of PU/montmorillonite is

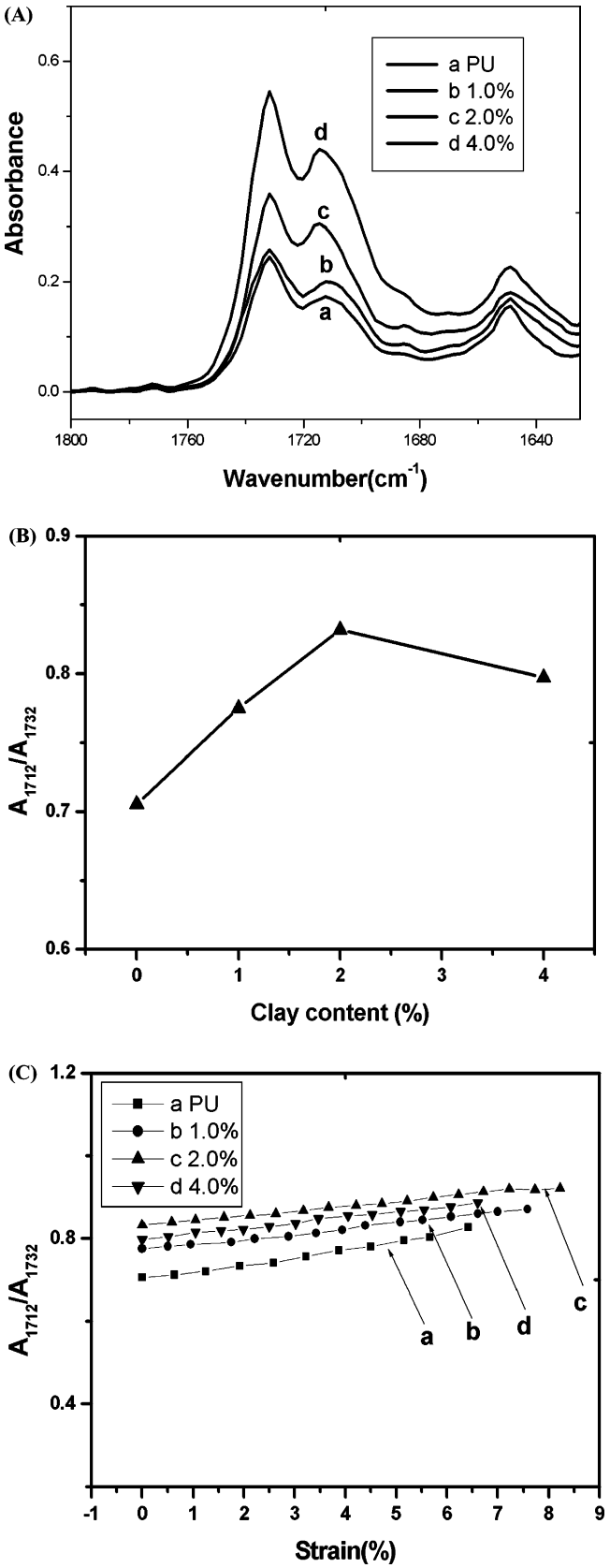


**Figure 9.** (A) IR stretching band of carbonyl group and (B) hydrogen-bonding index of urethane carbonyl vs clay contents before elongation. (C) Hydrogen-bonding change in stretching PU and PU/montmorillonite nanocomposites vs clay contents.

improved (shown in Figure 4). Upon stretching the hydrogen bonding increases very slowly for all samples. It is clear that there was a small increase of inter-

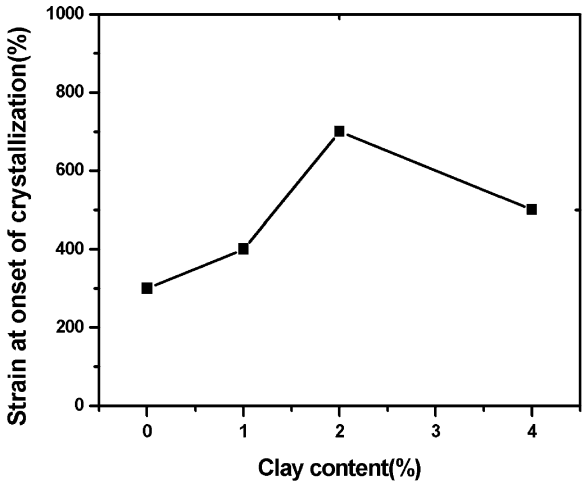


**Figure 10.** Strain at onset of crystallization vs clay content when soft segment chain crystallization induced by strain for PU and its nanocomposites.

urethane hydrogen bonding with elongation. A few hydrogen bonds are possibly disrupted when the material is extended. On the contrary, the macromolecular chains become more ordered along the strain direction during stretching. There appear more function groups such as C═O, N−H, and O−H, which could be shielded in the coiled molecular chains before stretching. In fact, the soft segment content in this system is about 80%, and the macromolecular chains are mostly coiled in an irregular mode under the no stretching state. So the probability of forming hydrogen bond increases. In Figure 9C, the whole change trend of hydrogen bonding increases slowly with samples stretching in PU and PU/clay composites, but in pure PU the increasing trend is faster than the other PU/clay composites. Also from Figure 9C, the addition of 2.0 wt % clay clearly causes a slowest increasing magnitude in hydrogen bonding of urethane carbonyl. This action well accorded with the results of the orientation of the hard segments of materials. (For sample II in Figure 7B,C, an increase of $f_{1712}/f_{1732}$ is smallest.) On further stretching, it could be supposed that formation of crystallite of the soft segments (shown in Figure 10) or formation of long-range ordered hard segments, which was similar to over cross-linked, and it would cause the break of materials. However, as the change of hydrogen bond of the material is relatively small, sample II could bear more stretching in Figure 9, which is similar to properly increase the physical cross-linking effects.

**Soft Segment Chain Crystallization Induced by Strain.** The soft segment crystallization depended on stretching also must be considered. The band at 997 $cm^{-1}$ is due to the symmetrical stretching vibration mode of C−O−C group in the PTMG chain. The band appears when the samples crystallized.[40,41] Thus, it can be used as a characteristic band to monitor the crystallization of soft segment chain in strain process. As stretching the specimen, this characteristic band appeared at elongation ratios in pure PU and PU/montmorillonite composites, as shown in Figure 10. The critical point of crystallization depends on multiple factors, such as temperature, strain, silicate layer content, and the relative content of hard segment and its chemical structure in the copolymers. In this study, one key factor is the content of clay. It is interesting that the strain values for the onset of crystallization of the soft segments increased with amount of clay at

beginning. When the content of clay is 2.0%, the strain value for the onset of crystallization was the highest about 700% in Figure 10. It means that the crystallization rate of soft segment decreased with increase the content of clay. The rate is slowest as the clay content is 2.0%. This trend is well accord with the orientation of the soft segment (shown in Figure 6). These results can be explained as follows. With elongating the sample the soft segments of PU were oriented along the strain direction. However, the crystallization of the soft segments induced by the stress is impeded by the organic montmorillonite, which is in accord with the results about the orientation of $f_{2940}$. It is evident that the introduction of nanoscale montmorillonite results in the suppression of the movement of molecular chains (the lamellar spacing of montmorillonite confines the molecular chain movement; also the hydrogen bonding slows down the movement of phase domains), which reduces the tendency for molecular chains to crystallize under the external strain. Moreover, the nanoscale montmorillonite is certain to have an "impurity" effect on the integrity of crystal lattices. Both of these lead to the decreasing of the rate of crystallization. Because of the decreasing of the rate of crystallization, sample II can markedly improve the elongation at the break, about 1700%. In short, the combination of the reinforcing effect of the silicate layers and its effect on the morphology of PU resulted in an optimal enhancement of the elongation at break with introducing the nanoscale montmorillonite.

## Conclusions

XRD, TEM, IR dichroism, and DSC experiments were carried out to characterize the morphology and properties of polyether polyurethane/montmorillonite composites. The microstructure and interaction of the macromolecular chains in the composites, such as orientation, hydrogen bonding, and crystallization induced by strain, were respectively studied. The PU/montmorillonite (2.0 wt %) sample exhibited a higher elongation at break than the other samples due to the exfoliated clay.

**Acknowledgment.** The 973 Program (No. 2003CB615600), National Natural Science Foundation of China (Grant No. 50373049), National 863 Project (No. 2001AA334060), and Key Project of CAS (KJCX2-SW-H07) are gratefully acknowledged for the financial support to this work.

## References and Notes

(1) Bayer, O. *Mod. Plast.* **1947**, *24*, 149.
(2) Okada, A.; Kawasui, M. *Polym. Prepr.* **1987**, *28*, 447.
(3) Vaia, R. A.; Ishii, H.; Giannelis, E. P. *Chem. Mater.* **1993**, *5*, 1694.
(4) Messersmith, P. B.; Giannelis, E. P. *Chem. Mater.* **1994**, *6*, 1719.
(5) Giannelis, E. P. *Adv. Mater.* **1996**, *8*, 29.
(6) Lan, T.; Kaviratna, P. D.; Pinnavaia, T. J. *Chem. Mater.* **1994**, *6*, 573.
(7) Vaia, R. A.; Vasudevan, S.; Krawiec, W.; Scanlon, L. G.; Giannelis, E. P. *Adv. Mater.* **1995**, *7*, 154.
(8) Pinnavaia, T. J. *Science* **1983**, *220*, 365.
(9) Wang, Z.; Pinnavaia, T. J. *Chem. Mater.* **1998**, *10*, 3769.
(10) Carsten, Z.; Ralf, T.; Rolf, M.; Jiirgen, F. *Adv. Mater.* **1999**, *11*, 49.
(11) Chen, T. K.; Tien, Y. I.; Wei, K. H. *Polymer* **2000**, *41*, 1345.
(12) Tortora, M.; Gorrasi, G.; Vittoria, V.; Galli, G.; Ritrovati, S.; Chiellini, E. *Polymer* **2002**, *43*, 6147.
(13) Sung, C. S. P.; Smith, T. W.; Sung, N. H. *Macromolecules* **1980**, *13*, 117.
(14) Meuse, C. W.; Yang, X.; Yang, D.; Hsu, S. L. *Macromolecules* **1992**, *25*, 925.
(15) Wang, C. B.; Cooper, S. L. *Macromolecules* **1983**, *16*, 775.
(16) Okada, A.; Kawasumi, M. *Mater. Res. Soc. Proc.* **1990**, *171*, 45.
(17) Zbinden, R. *Infrared Spectroscopy of High Polymers*, 2nd ed.; Academic Press: New York, 1969.
(18) Siesler, H. W.; Holland-Moritz, K. *Infrared and Raman Spectroscopy of Polymers*; Dekker: New York, 1980.
(19) Seymour, R. W.; Estes, G. M.; Cooper, S. L. *Macromolecules* **1970**, *3*, 579.
(20) Tien, Y. I.; Wei, K. H. *Polymer* **2001**, *42*, 3213.
(21) Tyan, H. L.; Liu, Y. C.; Wei, K. H. *Polymer* **1999**, *40*, 4877.
(22) Lan, T.; Kaviratna, P. D.; Pinnavaia, T. J. *Chem. Mater.* **1995**, *7*, 2144.
(23) Vaia, R. A.; Jandt, K. D.; Kramer, E. J.; Giannelis, E. P. *Chem. Mater.* **1996**, *8*, 2628.
(24) Chen, G. M.; Qi, Z. N.; Wang, F. S. *Polym. Bull. (Berlin)* **1999**, *4*, 3.
(25) Garrett, J. T.; Lin, J. S.; Runt, J. *Macromolecules* **2002**, *35*, 161.
(26) Theng, B. K. G. *Formation and Properties of Clay-Polymer Complexes;* Elsevier: New York, 1979.
(27) Chen, G. M.; Qi, Z. N.; Shen, D. Y. *J. Mater. Res.* **2000**, *15*, 351.
(28) Yeh, J. M.; Liou, S. J.; Lin, C. Y.; Cheng, C. Y.; Chang, Y. W. *Chem. Mater.* **2002**, *14*, 154−161.
(29) Lu, H. B.; Nutt, S. *Macromolecules* **2003**, *36*, 4010.
(30) Shen, Z. Q.; Simon, G. P.; Cheng, Y. B. *Polym. Eng. Sci.* **2002**, *42*, 2369.
(31) Zhao, Q.; Samulski, E. T. *Macromolecules* **2003**, *36*, 6967.
(32) Ishihara, H.; Kimura, I.; Saito, K.; Ono, H. *J. Macromol. Sci., Phys.* **1974**, *B10*, 591.
(33) Miller, C. E.; Edelman, P. G.; Ratner, B. D. *Appl. Spectrosc.* **1990**, *44*, 581.
(34) Lee, H. S.; Wang, Y. K.; Hsu, S. L. *Macromolecules* **1987**, *20*, 2089.
(35) Luo, N.; Wang, D. N.; Ying, S. K. *Polymer* **1996**, *37*, 3577.
(36) Luo, N.; Wang, D. N.; Ying, S. K. *Polymer* **1996**, *37*, 3045.
(37) Coleman, M. M.; Lee, H. H.; Skrovanek, D. J.; Painter, P. C. *Macromolecules* **1986**, *19*, 2149.
(38) Coleman, M. M.; Skrovanek, D. J.; Hu, J. B.; Painter, P. C. *Macromolecules* **1988**, *30*, 1234.
(39) Harthcock, M. A. *Polymer* **1989**, *30*, 1234.
(40) Imada, K. J. *Chem. Phys.* **1965**, *42*, 2807.
(41) Wen, Z. Q.; Shen, D. Y.; Zhao, H. Q. *Chin. J. Polym Sci.* **1988**, *64*, 325.

MA049900G